Elongational flow-induced birefringence of polyacrylamide and poly(acrylamide-*co*-sodium acrylate)

R. S. Farinato
American Cyanamid Company, 1937 West Main Street, Stamford, CT 06904, USA
(Received 16 February 1988; revised 28 April 1988; accepted 14 May 1988)

Aqueous solutions of poly(acrylamide-*co*-sodium acrylate), in up to 1 M NaCl, exhibited a flow-induced negative birefringence above a critical elongation flow rate in a crossed-slot device. Aqueous polyacrylamide, on the other hand, exhibited a positive birefringent pattern just above a critical elongation rate. At slightly higher elongation rates a negative birefringent thin-line region centred in the positive birefringent region appeared. This phenomenon was observed for all polyacrylamide concentrations tested (0.001 to 0.5 wt%; 0.5 to 20 times the quiescent overlap concentration). This change in birefringence sign can be qualitatively mimicked using a simple coil deformation model which includes contributions from intrinsic, microform and macroform optical anisotropy terms. Evidence is also given for this alternating birefringence sign pattern possibly being due to an elongational flow-induced change in the microstructure of the polyacrylamide.

(Keywords: elongational flow; birefringence; polyacrylamide; hydrolysed polyacrylamide; hydrogen bonding)

INTRODUCTION

The use of elongational flow birefringence for investigating the physical chemistry of macromolecules in solution has been steadily developing over the last decade[1–5]. Optical measurement of the process of polymer deformation and alignment in elongational flow fields has yielded information on the solution dynamics of both flexible and rigid polymers. By using appropriate hydrodynamic models, this dynamical information has also been used to determine molecular weights and molecular-weight distributions of high-molecular-weight polymers. Among its various applications to the physical chemistry of macromolecules in solution, the elongational flow birefringence method has been used to assess the scaling behaviour of polymer relaxation times with molecular weight[6–9] and polymer concentration[10], the kinetics of flow-induced chain scission[11,12], the effect of solvent quality and ionic strength on polymer dynamics[7,13] and the change in local polymer conformation due to the action of the flow field[1]. These experimental efforts have been paralleled by theoretical developments in the dynamics of macromolecules in elongational flow[14–16].

While fundamental information on chain dynamics is still being gathered in elongational flow birefringence experiments, the potential for information about the polymer microstructure, especially as it is influenced by the flow field, is beginning to be realized. As one example of this microstructural information, Keller and Odell[1] have explained certain features of the birefringence vs. strain rate curve and the appearance of a fine structure (of opposite birefringence sign) in the opposed-jet birefringence pattern for atactic polystyrene (3×10^6 daltons) in decalin as representing a flow-coupled rotation of the pendant phenyl groups.

In this paper we report on the fine structure in crossed-slot elongational flow birefringence patterns for aqueous polyacrylamide (PAM). These birefringence patterns are compared with those for hydrolysed polyacrylamide (HPAM or poly(acrylamide-*co*-sodium acrylate)). We show how this fine structure for PAM can yield microstructural information. The experimental manifestation of the fine structure was superficially quite similar to that reported by Keller and Odell[1] (i.e. a localized region of opposite sign of the birefringence). However, there were important differences in the phenomenon which are discussed below.

EXPERIMENTAL

Polymer solutions

All the polymers were made at American Cyanamid Co. using a free-radical procedure. Hydrolysis was with NaOH. The extent of hydrolysis was determined using infra-red spectroscopy. Polymer properties are listed in *Table 1*. All polymers were dissolved in water purified first by deionization, then a reverse osmosis treatment

Table 1 Polymer properties

	PAM1	HPAM1	HPAM2
$[COO^-]$ (mol%)	0	30	14
$[\eta]$ (dl g^{-1}) at 25°C			
in water	41.0		
in 1 M NaCl		25.1	
Molecular weight $\times 10^{-6}$	25.3[a]	10.1[b]	
(viscosity average)		5.4[c]	

[a] Mark–Houwink coefficients interpolated from Klein and Conrad[19] (water)
[b] Mark–Houwink coefficients interpolated from McCarthy *et al.*[39] (1 M NaCl)
[c] Mark–Houwink coefficients interpolated from Klein and Conrad[19] (0.5 M NaCl)

0032-3861/88/122182-09$03.00

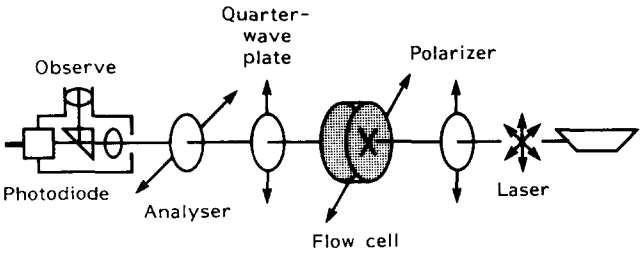

Figure 1 Schematic of elongational flow birefringence experiment

(MilliQ, Millipore Corp., Bedford, MA) and finally by filtration (0.2 μm, Nucleopore Corp., Pleasanton, CA). Any electrolyte was added in the initial polymer dissolution process. Solutions were placed in capped glass jars and rolled at least overnight at room temperature. If subsequent dilutions were made, the solution was further rolled for an additional day. The polymer solutions were slowly ($\sim 21\,h^{-1}$) filtered (8 μm Nucleopore) just prior to use. The polymer solutions were usually aged a minimum of 1–2 weeks before birefringence experiments were performed. No bacterial action was evidenced during that period.

Elongational flow birefringence

The apparatus, based on a crossed-slot design, has been described previously in detail[17]. A schematic of the experiment is shown in *Figure 1*. The polymer solution flowed from a helium-pressurized stainless-steel reservoir through opposing arms of a crossed-slot configuration formed from four optical-quality prisms with a hydrophobic coating (Nyebar, W. F. Nye Corp., New Bedford, MA). The prism faces were 25 mm × 25 mm and were held 2 mm apart in a rigid holder made of Delrin. The prisms were sealed to 1/4 inch thick optical flats on either side. These flats provided for low residual birefringence entrance and exit windows for the polarized light beam. The solution exited out the other two opposing arms of the flow cell and its volume flow rate was controlled by a valve at the very end of the hydraulic system. The gravimetric flow rate q of a solution of density ρ_s was used to calculate the nominal strain rate $\dot{\varepsilon}$ according to:

$$\dot{\varepsilon} = \langle v \rangle / B = q/(4\rho_s B^2 W) \quad (1)$$

where $\langle v \rangle$ is the average fluid velocity through the slots of depth W separated by a distance $2B$. The polymer relaxation time τ_{efb} was calculated from the critical strain rate $\dot{\varepsilon}_c$ for the appearance of birefringence:

$$\tau_{efb} = 1/\dot{\varepsilon}_c \quad (2)$$

The critical onset flow rate for flow-induced birefringence was determined either from the transmitted light intensity measured with a photodiode, or directly from the visualizations on video camera. Because of the small inherent birefringence of polyacrylamides (see below), working off the crossed polarizer/analyser position increased the sensitivity. By using a 12 dB gain enhancement mode on the video camera with the off-crossed polarizer/analyser configuration, the critical onset points were most easily determined directly in the visualization mode. Critical velocities were reproducible to about 10% using this method.

The pressure drop δP across the flow cell was recorded simultaneously with the transmitted light intensity signal. The polymer solutions passed only once through the flow cell since flow through the exit valve tended to degrade the molecular weight of the polymers. This was evidenced by a reduced birefringence signal and an increase in the onset strain rate for second-pass solutions. Each measurement was made under steady-state conditions. Flow instabilities eventually occurred as the flow rate increased; however, the viscoelastic character of even the dilute polyacrylamide solutions tended to stabilize the flow patterns against minor irregularities. Under equivalent conditions it was noted that the HPAM flow birefringence patterns were not nearly as stable as those for PAM.

The optical train included a quarter-wave plate (mica; optimized for 632.8 nm; slow axis oriented vertically) between the flow cell (flow exit axis at $-45°$ from the vertical when viewed into the beam) and the analyser to allow determination of the sign of the birefringence. The polarizer (oriented vertically) and analyser (oriented near the horizontal) were sheet dichroics with an extinction ratio of $\sim 10^{-3}$. They were normally operated in the off-crossed position (typically $\pm 5°$). The angles of optical elements designated in this paper (see *Figure 2*) were measured as positive anticlockwise from the vertical (0°) looking into the beam. The offset angle α of the analyser from the horizontal position (90°) was measured as positive clockwise looking into the beam. Thus the angular position of the analyser was $90° - \alpha$. This is the convention used by Fredericq and Houssier[18].

The birefringence signals with polarizer and analyser in the crossed position for the polyacrylamide polymers studied were small (see discussion below) and could be easily missed. This underscored the need for the enhanced sensitivity obtained in using the quarter-wave plate and the slightly off-crossed polarizer/analyser combination. The magnitude of the birefringence, Δn, which is the difference between the refractive indices for light polarized parallel and perpendicular to the flow exit axis, was directly proportional to the difference in transmitted light intensity (with and without flow) since we were using a quarter-wave plate[18].

For direct observation and recording of the flow birefringence pattern, a focused tungsten or a flash lamp source was used. The images were recorded either with a Sony WV 555B video camera (tungsten source) or a Nikon F3 camera with a 105 mm Micro-Nikkor lens (Speedatron flash lamp source). For quantitative

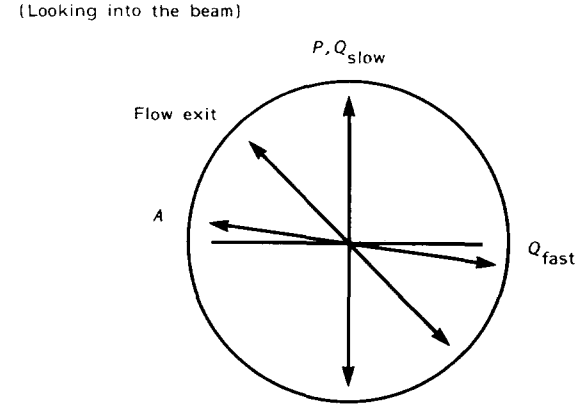

Figure 2 Optical axes of elements in elongational flow birefringence experiment

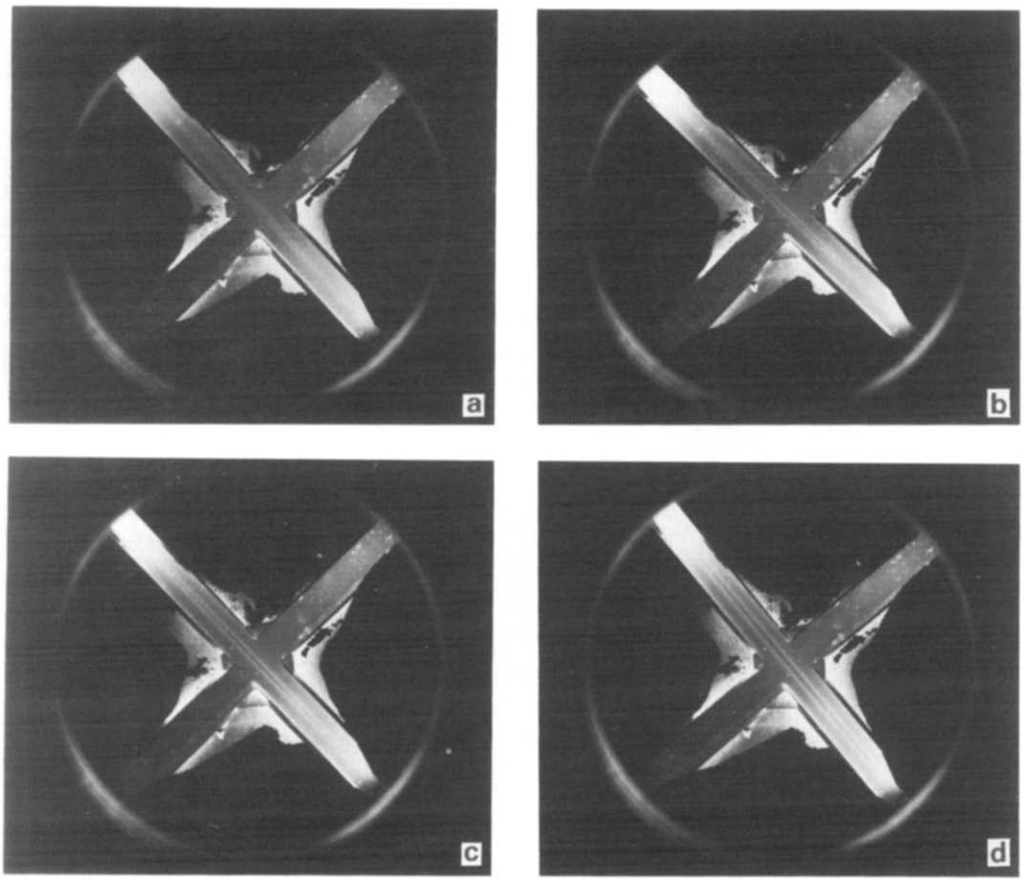

Figure 3 Elongational flow birefringence patterns for 0.2 wt% aqueous PAM1 at pH 5.5. Analyser angle $A=95°$ ($\alpha=-5°$); light increase = (+) birefringence; light decrease = (−) birefringence. Flow velocity (cm s^{-1}) was: (a) 5.41, (b) 7.76, (c) 9.95 and (d) 16.34. Nominal $\dot{\varepsilon}$ were 10 times flow velocities

determinations of the birefringence, an unfocused 5 mW HeNe laser (Hughes) was used as the light source and a silicon photodiode (United Technologies PIN-10DF with a 101C amplifier) as the detector.

Intrinsic viscosity

Flow times in four-bulb Cannon Ubbelohde capillary viscometers were used to determine the intrinsic viscosity $[\eta]$ for the polymers at zero shear rate. At least five points were within the linear region of the specific viscosity vs. polymer concentration plots. The results are shown in *Table 1*. The polymer relaxation time τ_{iv} at a temperature T (K) was calculated as the lowest normal-mode Rouse relaxation time:

$$\tau_{iv}=[\eta]\eta_s M/(N_A k_B T) \quad (3)$$

for a solvent viscosity η_s and a polymer molecular weight M. The other symbols in equation (3) are for Avogadro's number N_A and the Boltzmann constant k_B. The polymer molecular weight used in equation (3) was calculated from the Mark–Houwink relation, $[\eta]=KM^a$, where the Mark–Houwink coefficients K and a determined by Klein and Conrad and by McCarthy *et al.*[19] were used.

RESULTS

Flow visualizations

Polyacrylamide. The flow-induced birefringence pattern for non-ionic polyacrylamide appeared as a stable thin line along the exit channels of the crossed-slot flow cell above a critical strain rate $\dot{\varepsilon}_c$. This pattern, which was positive birefringent, was best seen with the polarizer and analyser off the crossed position. At strain rates $\dot{\varepsilon}_*$ slightly larger than $\dot{\varepsilon}_c$, the birefringent line developed a well demarcated fine structure consisting of a central line of negative birefringence surrounded by two lines of positive birefringence (+/−/+). *Figure 3* shows a series of these patterns for 0.2 wt% PAM1 (pH 5.5) at increasing flow rates. The analyser was 5° clockwise from the crossed position ($A=95°$; $\alpha=-5°$) which resulted in a lighted background. For the optical configuration used in these experiments and $\alpha<0$, a negative birefringence appeared as a decrease in transmitted light intensity and a positive birefringence appeared as an increase in light intensity. By turning the analyser to the opposite side of the crossed position ($\alpha>0$) the background would still be lighted, but a negative (positive) birefringence produced an increase (decrease) in light intensity. This fact was used to assure that the light/dark patterns were due to an induced birefringence and not to a concentration or thermal gradient effect. Also, by changing the magnitude of α and observing the same light/dark patterns we were assured that a birefringence sign reversal due to a retardation larger than $|\alpha|$ was not occurring. *Figure 4* shows the reversal (light ↔ dark) in the birefringence patterns for the same polyacrylamide homopolymer as in *Figure 3* (0.2 wt%, pH 5.5) with the analyser 5° anticlockwise off crossed ($A=85°$ $\alpha=+5°$).

The +/−/+ fine structure was seen in non-ionic polyacrylamide samples at all concentrations tested, from

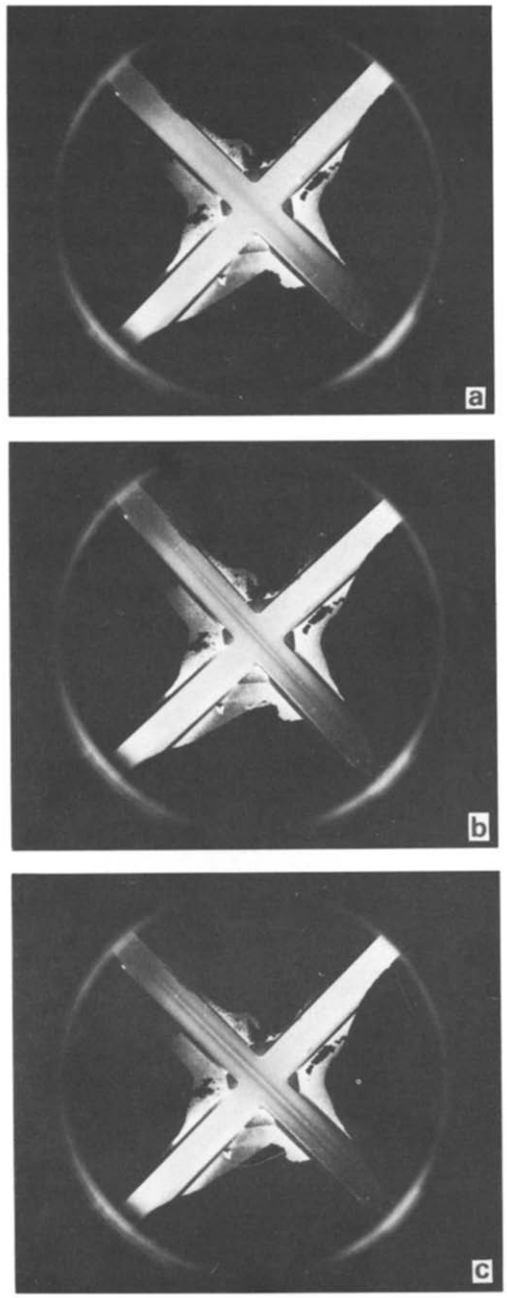

Figure 4 Elongational flow birefringence patterns for 0.2 wt% aqueous PAM1 at pH 5.5. Analyser angle $A = 85°$ ($\alpha = +5°$); light increase = (−) birefringence; light decrease = (+) birefringence. Flow velocities (cm s^{-1}) were: (a) 4.24, (b) 9.73 and (c) 17.46. Nominal $\dot{\varepsilon}$ were 10 times flow velocities

0.001 to 0.5 wt%. Recording the visualizations at concentrations lower than 0.001 wt% was difficult with the present quality of the optics. Estimating the overlap concentration as $c^* = 1/[\eta]$ gave $c^* = 0.024\ wt\%$ for PAM1. Thus we saw the fine structure at polymer concentrations from about 0.5 to 20 times the quiescent overlap concentration, the entire range tested.

A closer inspection of *Figures 3* and *4* showed that the central and total linewidths increased regularly with flow rate. *Figure 5* is a plot of the central and total birefringent linewidths vs. the flow rate. The linewidths were measured (±0.02 mm) directly from enlarged photographs. To a first approximation the central and total linewidths increased linearly with flow rate. The central birefringent line appeared at a critical flow (elongation) rate v_* ($\dot{\varepsilon}_*$), which was slightly larger than the critical onset rate for birefringence. The rate of birefringence linewidth increase with flow rate was approximately twice as great for the total linewidth as for the central linewidth.

As mentioned above, the flow-induced birefringence patterns were very stable up to a flow rate where inertial effects created a chaotic flow field. Even at the highest polymer concentrations tested, there was never any evidence of flaring birefringent patterns as have been seen for polystyrene and poly(ethylene oxide)[9] and which have been interpreted as being due to a molecular connectedness in a flow-induced network at semi-dilute polymer concentrations. Also conspicuously absent in the visualizations was the presence of any dramatic stationary wall-induced birefringence as has been seen in atactic polystyrene[20], poly(styrene sulphonate)[17] and xanthan[21]. This was attributed to the small optical anisotropy of PAM.

The qualitative features of the +/−/+ birefringence fine structure was not dramatically affected by the PAM concentration over the range tested, except in overall intensity. However, changing the solvent did dramatically affect the fine structure. Whereas an aqueous 0.05 wt% PAM1 solution clearly exhibited the +/−/+ fine structure, the same polymer concentration in a 40 wt% aqueous glycerol solution did not. A single thin localized negatively birefringent line was seen for PAM in 40% glycerol.

Hydrolysed polyacrylamide. HPAM1 (30% acrylate) was investigated over a range of aqueous NaCl solutions (50 μM–1 M), whereas HPAM2 (14% acrylate) was investigated only in 50 μM NaCl. Operating over the same polymer concentration range as for the non-ionic PAM1 homopolymer, stable birefringence patterns with aqueous and salt solutions of HPAM1 and HPAM2 were difficult to achieve with the present size of flow cell. A relatively stable flow pattern resulted with the 30 mol% acrylate copolymer in 1 M NaCl. In this case the sample exhibited a simple thin-line flow-induced birefringence pattern with no fine structure. The sign of the birefringence was negative and showed a critical onset strain rate. All of the observed flow-induced birefringence for the acrylamide–sodium acrylate copolymers in aqueous salt solutions had a negative sign.

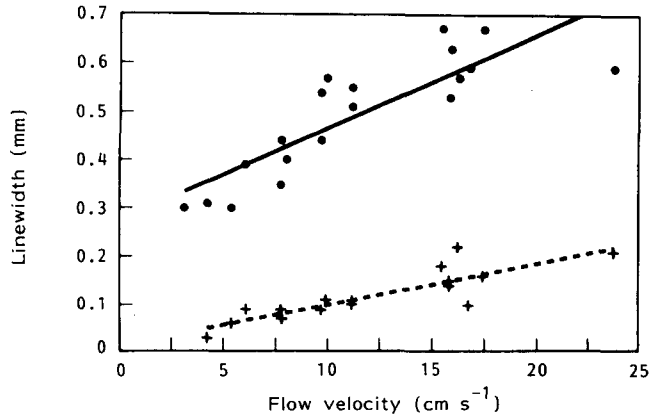

Figure 5 Width of total (●) and central (+) birefringent lines vs. flow rate for 0.2 wt% aqueous PAM1 at pH 5.5

Relaxation times

The polymer relaxation times τ_{efb} were calculated from the onset flow velocities using equations (1) and (2). The value of τ_{efb} for 0.2% PAM1 in water was 48 ms and for 0.1% HPAM1 in 1 M NaCl was 40 ms. No attempt was made in this study to extrapolate τ_{efb} values to zero polymer concentration, so they cannot strictly be compared with relaxation times from intrinsic viscosity.

DISCUSSION

Elongational flow birefringence sign changes

The observations for PAM and HPAM can be summarized as follows:

(i) For a high-molecular-weight PAM in water (pH 5.5), the critical onset of a thin centrally located line (along the exit flow axis) of positive birefringence occurred at $\dot{\varepsilon}_c$; the width of the birefringent line was approximately linear with flow velocity.

(ii) At a second slightly larger critical strain rate $\dot{\varepsilon}_*$, a thin centrally located line of negative birefringence appeared within the positive birefringent region; the width of this negative birefringent region increased linearly with flow velocity. This phenomenon was seen at all concentrations of PAM investigated (0.001–0.5 wt%), above and below the quiescent c^*.

(iii) PAM1 dissolved in 40% aqueous glycerol exhibited only a negative birefringent thin line above a critical flow rate; no positive birefringent region was seen at any flow rates.

(iv) Birefringent patterns for PAM1 were very stable.

(v) All HPAM solutions (0.003–0.1 wt% polymer; 50 μM–1 M NaCl) exhibited only a negative birefringence; the birefringent regions were not very stable.

There have been several previous reports of fine structure in elongational flow birefringence patterns similar in appearance to the type seen in this work. In opposed-jet experiments this fine structure had a tubular appearance. Odell and Keller[11] demonstrated such an effect in atactic polystyrene in decalin. A weakly positive birefringence in the central region connecting the opposed jets was surrounded by a concentric negatively birefringent region. However, this phenomenon was seen only above a certain polymer concentration and at high strain rates. This is in contrast to the effect for polyacrylamide reported here, where the fine structure was seen over a wide range of concentrations, above and below the quiescent critical overlap concentration, and at all strain rates above $\dot{\varepsilon}_*$. Odell and Keller[11] also reported fine structure in samples of aqueous poly(ethylene oxide), but again only at high polymer concentrations. In the case of polystyrene, the birefringence fine structure was interpreted in terms of a flow-coupled rotation of the pendant phenyl groups. In the case of poly(ethylene oxide), intermolecular interactions were implicated.

Concentric fine structure in opposed-jet birefringence could result in another way. Regions in the flow cell of sufficiently high flow rates would randomize the orientation of the macromolecules. Since flow rates would be highest along the centreline in opposed-jet or crossed-slot configurations, a visualization of the birefringence pattern would show a concentric structure for this case. This type of behaviour would occur at a critical flow rate much larger than for the onset of birefringence. Also, in this case, the magnitude of the birefringence in the high-flow-rate regions would be near zero and not necessarily of the opposite sign to the other birefringent regions. Examples of this type of fine structure have been reported by Peiffer *et al.*[13] and Cressely *et al.*[22]. In all of the examples of our work reported here the flow rates were low enough to avoid these high-flow-rate effects. Typically our nominal Reynolds numbers ($Re \approx 4\dot{\varepsilon}\rho_s B^2/\eta$) were less than 500. By going to higher flow rates it was possible to generate birefringence patterns which included a confined chaotic region of diminished birefringence magnitude.

Another mechanism that could produce a concentric fine structure in elongational flow birefringence is flow-induced degradation of the polymer. This effect would be most severe at the stagnation point (centre of the flow cell) and along the centreline of the exit flow channels. The susceptibility of polyacrylamide to elongational flow-induced degradation is well known, and in multiple passes of the same polyacrylamide solution through our flow cell the birefringence signal became progressively weaker with each pass. However, these repeated passes did not alter the +/−/+ birefringence pattern. For molecular-weight degradation we would expect the magnitude of the birefringence to decline, but there should be no change in the sign of the birefringence. We minimized the effects of molecular-weight degradation by passing the solutions through the flow cell only once, even though molecular-weight degradation was not responsible for the alternating sign of the birefringence seen in the central region of the flow cell.

Both the linear elongation rate dependence of the width of the central birefringent region (*Figure 5*) and the sign reversal of the birefringence (*Figures 3* and *4*) suggested a flow-coupled microstructural change in the polyacrylamide. The fact that the fine structure was not seen with either the acrylamide–acrylate copolymer or with PAM in a thermodynamically poorer solvent (aqueous glycerol) suggested the phenomena may be related to the hydrogen-bonding structure of the polymers in solution.

Hydrogen bonding in PAM and HPAM

Polyacrylamide and poly(acrylamide-*co*-sodium acrylate) both show a propensity for intramolecular hydrogen bonding. Klein and Scholz[23] reported calorimetric evidence for the specific interaction of neighbouring carboxylate and amide groups in a poly(acrylamide–sodium acrylate) copolymer. Kulicke and Kniewske[24,25] showed that intramolecular hydrogen bonding in polyacrylamide and poly(acrylamide-*co*-sodium acrylate) led to long-term conformational changes in high-molecular-weight samples of the polymers. They postulated several types of intramolecular hydrogen bonds for these polymers in their freshly dissolved states. These structures rearranged continuously over a period of about 1 month in solution to include only bridging between non-neighbouring chain units (Z-type hydrogen bonding in Kulicke and Kniewske's scheme). This resulted in a minimization of ordered chain segments. In this type of arrangement the hydrogen bonds were predominantly perpendicular to the local chain axis. Hydrogen bonds between neighbouring chain units in ordered segments (stiff linear and helical regions), found in freshly dissolved polymer, were oriented predominantly parallel to the local chain axis.

The solution conformation of polyacrylamide has been

reported to be affected by the addition of hydrogen-bond-moderating additives[25,26]. Glycerol (0.5 M), for example, increased the intrinsic viscosity of a polyacrylamide solution over a period of 2 weeks by promoting hydrogen bonding, presumably between neighbouring chain units to produce stiffer ordered segments[25].

Optical anisotropy of flexible macromolecules

The birefringence Δn of polymers in flow arises from two contributing factors[27,28]: an optical anisotropy $(\gamma_1-\gamma_2)$ and an orientation function $f(p, \sigma, t_{tr})$:

$$\Delta n=\frac{2\pi C}{n}(\gamma_1-\gamma_2)f(p, \sigma, t_{tr}) \quad (4)$$

where C is the concentration (particles/cm^3) and n is the solution refractive index. For elongational flow experiments the orientation function depends on: (1) the anisometry of the particle (p = major/minor axis length), which can be either intrinsic (i.e. rigid particles) or induced by deformation under flow; (2) the reduced strain rate ($\sigma=\dot{\varepsilon}/D_r$; D_r = rotational diffusion constant); and (3) the transit time t_{tr} in the flow field.

The optical anisotropy factor is composed of three terms for flexible molecules: (1) the intrinsic anisotropy of a chain segment, (2) a short-range optical interaction which leads to a local anisotropy of the polarizing field due to the asymmetrical distribution of neighbouring elements (microform effect) and (3) a long-range optical interaction due to a non-spherical distribution of chain elements which also results in an anisotropy of the polarizing field within the molecule (macroform effect). All three terms are functions of the deformation of the macromolecule. Tsvetkov[27,29] has discussed these contributions with regard to macromolecular deformation and orientation in shear flows. Since in shear flows the deformations are small, he discussed mainly the small-deformation limits of flow-induced birefringence. However, the expressions for the large-deformation case (as expected in elongational flows) are implicit in his basic equations. We outline this extension below.

As a chain model Tsvetkov[27,29] used the freely jointed chain of Kuhn and Grun[30] in a coordinate system related to the end-to-end vector **h**. For a chain of contour length L, the optical anisotropy of the entire chain was given by:

$$(\gamma_1-\gamma_2)=\left(\frac{n_s^2+2}{3}\right)^2\{(\delta\alpha_i+\delta\alpha_{fs})L[1-3x/L^*(x)] + \delta\alpha_f(L_2-L_1)\} \quad (5)$$

where n_s is the solvent refractive index, $\delta\alpha_i$ is the intrinsic optical anisotropy of the monomer, $\delta\alpha_{fs}$ is the microform anisotropy and $\delta\alpha_f$ is the macroform anisotropy (see below). $L^*(x)$ is the inverse Langevin function of x (x = the reduced length h/L) and h is the magnitude of the average end-to-end vector. The optical shape factor (L_2-L_1) is a function of $h/(h_0^2)^{1/2}$, where $(h_0^2)^{1/2}$ is the r.m.s. end-to-end distance of the undeformed chain. The optical shape factor was given as[31]:

$$(L_2-L_1)=\left(\frac{\pi}{p^2-1}\right)2p^2+4 - \left(\frac{3p}{(p^2-1)^{1/2}}\right)\ln\left(\frac{p+(p^2-1)^{1/2}}{p-(p^2-1)^{1/2}}\right) \quad (6)$$

For flexible chains:

$$p=[1+1.5(h^2)/(h_0^2)]^{3/4} \quad (7)$$

The intrinsic optical anisotropy per monomer, $\delta\alpha_i$, can be determined from flow or electric birefringence measurements, or it can be calculated from monomer geometry and bond optical polarizabilities. Note that $\delta\alpha_i$ can be positive or negative.

The microform anisotropy term is:

$$\delta\alpha_{fs}=\left(\frac{n_p^2-n_s^2}{4\pi n_s}\right)^2\left(\frac{M_0}{\rho_p N_A}\right)(L_2-L_1)_s \quad (8)$$

where n_p is the polymer refractive index, M_0 is the monomer molecular weight, ρ_p is the polymer density, N_A is Avogadro's number and $(L_2-L_1)_s$ is the segmental spatial asymmetry function, analogous to the optical shape factor. The microform anisotropy $\delta\alpha_{fs}$ is always positive.

The macroform anisotropy term is:

$$\delta\alpha_f=\left(\frac{n_p^2-n_s^2}{4\pi n_s\rho_p N_A}\right)^2\frac{M^2}{v} \quad (9)$$

where M is the polymer molecular weight and v is the chain volume, estimated as $0.36(h^2)^{3/2}$ (ref. 27). The macroform anisotropy is always a positive number.

Intrinsic optical anisotropy

The intrinsic optical anisotropy for PAM was not readily available in the literature. Kuhn *et al.*[32] determined the segment intrinsic optical anisotropy of NaPAA in 0.0012 M NaCl at pH 7 to be -20×10^{-25} cm^3 from shear flow birefringence measurements[33]. This number would have to be divided by the number of monomers per statistical segment to obtain the intrinsic optical anisotropy per monomer, $\delta\alpha_i$.

We made an estimate of $\delta\alpha_i$ using a vector addition of bond optical polarizabilities. A semiempirical quantum-mechanical package (CHEMLAB, Molecular Design Ltd, San Leandro, CA) was used to compute the minimum-energy conformation of the following trimer segments representative of the polymers studied: Am–Am–Am, Am–AA–Am and Am–Ac–Am (where Am = acrylamide, Ac = acrylate and AA = acrylic acid). A conformational energy minimization on a fixed valence geometry was used taking account of steric, electrostatic and hydrogen-bonding contributions to the energy. The charge on the acrylate ion was calculated using the CHEMLAB CNDO/2 package. The geometry of the middle monomer in each of the minimum-energy conformations were used to sum vectorially the bond optical polarizabilities (from refs. 34 and 35) and to compute the resultant intrinsic optical anisotropy $\delta\alpha_i$ as the difference between the optical polarizability parallel and perpendicular to the chain axis.

This intrinsic optical anisotropy calculation did not take into account electron density distributed into hydrogen bonds, or that due to the sodium counterion associated with the acrylate ion. Judging from optical anisotropy data on polyacrylates[33], the sodium counterion would be expected to make a negative contribution to the intrinsic optical anisotropy. For the hydrogen-bond contribution we have to consider several possiblities. The hydrogen bonds may be either intra- or intermolecular and they may be oriented parallel or perpendicular to

Table 2 Intrinsic optical anisotropies of monomers

Monomer	Formula	$\delta\alpha_i$ (10^{-25} cm^3)
Acrylamide	-($CH_2CHCONH_2$)-	$-8.0+H_a$
Acrylic acid	-($CH_2CHCOOH$)-	$-5.7+H_b$
Acrylate	-(CH_2CHCOO^-)-	$-2.0+H_c$

the local chain axis, as described above. For parallel orientations, such as would occur in ordered segments within the same molecule, the hydrogen bonds would make a positive contribution to $\delta\alpha_i$ (and Δn). This would be favoured in situations where the neighbouring group interactions were strongest (e.g. in the acrylamide/sodium acrylate copolymer at low polymer concentrations). Perpendicular orientation of the hydrogen bonds would make a negative contribution to $\delta\alpha_i$ (and Δn). According to the model of Kulicke and Kniewske[24,25], this would prevail in aged polyacrylamide and poly(acrylamide-*co*-sodium acrylate) solutions, and in situations that promoted intermolecular or non-neighbour intramolecular hydrogen bonding.

Extensional flows might be expected to produce two effects. For an isolated chain under extension, neighbouring hydrogen-bond formation (a positive contribution to $\delta\alpha_i$) might be more favourable than remote hydrogen bonding. However, if intermolecular hydrogen bonds were promoted between extended chains, this would result in a negative contribution to $\delta\alpha_i$.

Table 2 shows the results of the intrinsic optical polarizability calculations. For all these polyacrylamide type model trimers the optical bond polarizabilities (without the hydrogen-bonding contribution, H_i) nearly cancelled, resulting in a small negative $\delta\alpha_i$. This magnitude was consistent with the small birefringence signal and also the absence of any appreciable wall birefringence. Wall birefringence is due predominantly to deformations and/or alignment in shear fields. This is appreciable only when the polymer is rigid, prestretched or partially adsorbed, and has a significant optical anisotropy.

As a comparison, many proteins have 10–100 times the optical anisotropy per monomer unit as do these acrylamide copolymers. The data in *Table 2* suggest that the sign of the birefringence of polyacrylamide copolymers might be easily influenced by the prevailing state of hydrogen bonding in the polymer.

Optical anisotropy calculation

Figure 6 shows the total optical anisotropy for PAM1 as a function of the extension ratio h/h_0 over a reasonable range of $\delta\alpha_i$, including microform and macroform effects (equation (5)). The parameters used in these calculations were:

$$n_s = 1.33$$
$$n_p = 1.61$$
$$\rho_p = 1.302 \text{ g cm}^{-3}$$
$$M_0 = 71$$
$$M = 27.2 \times 10^6$$
$$h_0 = 9.49 \times 10^{-5} \text{ cm}^3$$
$$-1 \times 10^{-25} \text{ cm}^3 \geqslant \delta\alpha_i \geqslant -10 \times 10^{-25} \text{ cm}^3$$

and n_p was calculated from:

$$dn/dc = \tfrac{3}{2} v_2 n_s [(m^2-1)/(m^2+2)] \quad (10)$$

where $m = n_p/n_s$. We used $dn/dc = 0.187$ cm^3 g^{-1} and $v_2 = 0.693$ cm^3 g^{-1} (ref. 36); h_0 was calculated using[36]:

$$(h^2)_w^{0.5} = 0.39 M_w^{0.59} \quad (11)$$

where h is in angströms.

We see in *Figure 6* that there is a reasonable range of $\delta\alpha_i$ for which small amounts of deformation would cause a sign change in $(\gamma_1 - \gamma_2)$, and hence in Δn, from positive to negative as the extension ratio increased. This mimicked what was observed experimentally for aqueous PAM solutions in elongational flow when $\dot{\varepsilon} \geqslant \dot{\varepsilon}_*$, assuming the extension ratio to decrease moving from the centreline of the exit flow axis to the stationary walls.

As the $\delta\alpha_i$ term becomes more negative, the above model would predict only a negative birefringence in the flow-induced patterns, even for small deformations. This solely negative birefringence was the condition seen for the HPAM copolymers and the PAM1 in glycerol solutions. Although the bond optical polarizability calculations (*Table 2*) indicated the acrylate ion to have a smaller negative intrinsic optical anisotropy than the acrylamide monomer, this estimate did not take into account the effect of the sodium counterion, nor the stronger hydrogen bonds expected with the acrylate ion. It is quite possible that these two effects could make $\delta\alpha_i$ more negative for HPAM than for PAM.

The addition of glycerol ($n^D = 1.475$) to PAM solutions would have two effects. First, it would reduce the microform and macroform contributions to the optical anisotropy by simply increasing the solvent refractive index to values closer to the polymer refractive index. Secondly, glycerol would tend to promote hydrogen bonding since it is a worse solvent for the PAM than water. For aged solutions this would make $\delta\alpha_i$ more negative. Both effects would promote the appearance of only a negative birefringent line in elongational flow.

The above calculations, however, do not exclude the possibility of flow-induced changes in $\delta\alpha_i$ due to, for example, a repartitioning of hydrogen bonds in the flow-extended chains. In fact, the greater flow stability of the PAM1 birefringence patterns, even at low polymer

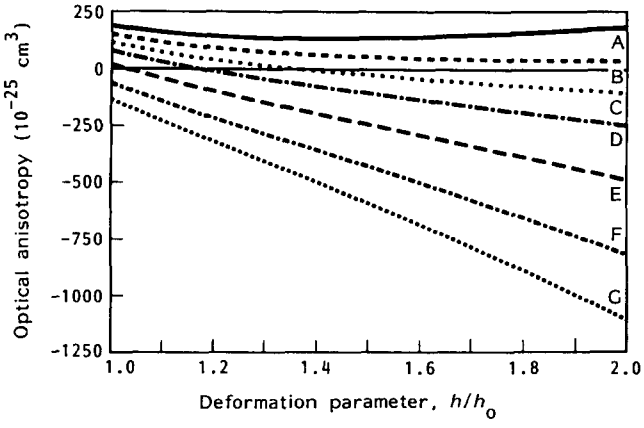

Figure 6 Optical anisotropy for a flexible chain vs. deformation parameter (h/h_0) calculated using equation (5). Intrinsic optical anisotropy term: −1 (A), −2 (B), −3 (C), −4 (D), −5.7 (E), −8 (F) and −10 (G) × 10^{-25} cm^3. Other parameters are given in the text

concentrations, suggested some enhanced intermolecular interaction of the elongated molecules.

Conformational change energetics

Assuming that a conformational change in PAM1 partly underlay the sign change of the birefringence at $\dot{\varepsilon}_*$, an estimate of the energy involved in this flow-induced PAM conformational change was made using the rotational isomeric state model of flexible coil stretching in elongational flow developed by Henyey and Rabin[37]. We used their dilute-solution non-free-draining model for the partially stretched coil as suggested by Dash *et al.*[38]. The energy difference ΔE (per mole) between the two states in this model at the strain rate ($\dot{\varepsilon}_*$) corresponding to the onset of the central negative birefringent region was solved for explicitly (from equation (35) in ref. 37):

$$\Delta E = -RT\ln\{N[(Cn_s l^3\dot{\varepsilon}_*)/(4.15k_BT)]^{2/3}\} \quad (12)$$

where R is the gas constant, T the temperature (K), N the number of monomers (each of length l) per chain, n_s the solvent viscosity, k_B the Boltzmann constant and

$$C = 2\pi/[\ln(Z/w)] \quad (13)$$

The chain is of length Z and width w. For the PAM used in this study:

$$N = 3.8 \times 10^5$$
$$Z = 9.6 \times 10^{-3}\ \text{cm}$$
$$w = 5 \times 10^{-8}\ \text{cm}$$
$$l = 2.5 \times 10^{-8}\ \text{cm}$$
$$n_s = 0.01\ \text{P}$$
$$T = 295\ \text{K}$$

resulting in:

$$\Delta E \approx -0.586\ln(0.00232\dot{\varepsilon}_*^{2/3})\ \text{kcal mol}^{-1}$$

For the PAM sample pictured in *Figures 3* and *4* (in the semi-dilute concentration range), $\dot{\varepsilon}_* \approx 50\ \text{s}^{-1}$ and $\Delta E \approx 2.0\ \text{kcal mol}^{-1}$. This is on the low side of typical hydrogen-bonding energies, but it must be recalled that not every monomer would be involved in a hydrogen bond with another chain segment. Since the statistics of the hydrogen bonding in solution PAMs is not known here, the above calculation remains only suggestive.

SUMMARY

High-molecular-weight PAM and HPAM in aqueous solutions both showed a critical onset of flow-induced birefringence (thin line centred in the exit flow channels) as expected for flexible polymers. Under all conditions examined (NaCl solutions), the HPAM exhibited only negative birefringence. PAM, on the other hand, exhibited a positive birefringence for strain rates just above the onset elongation rate ($\dot{\varepsilon}_c$). At a slightly higher critical elongation rate ($\dot{\varepsilon}_*$) there appeared a negative birefringent region, centred within the positive birefringent region. The appearance of this +/−/+ birefringence pattern occurred for all aqueous PAM concentrations studied (0.001 to 0.5 wt%), both above and below the quiescent overlap concentration. In a thermodynamically worse solvent (aqueous glycerol) the +/−/+ pattern reverted to a simple negative birefringent line. The width of both the positive and negative birefringent regions increased linearly with flow rate.

The birefringence as a function of elongation parameter was predicted from a simple deformation model of a flexible coil, which included intrinsic, microform and macroform optical anisotropy contributions. The predictions were qualitatively similar to the experimental observations for PAM over a narrow, but reasonable, range of intrinsic optical anisotropies.

Calculations suggested that PAM and HPAM should both have a small negative intrinsic optical anisotropy which should be senstive to the intra- and intermolecular hydrogen-bonding state of the molecule. Intermolecular and/or non-neighbouring intramolecular hydrogen bonding would make the intrinsic optical anisotropy more negative. Intermolecular hydrogen bonds could be promoted between flow-elongated chains.

The change in sign of the birefringence with elongation rate was also modelled as a conformational change. The energy associated with this change was calculated to be 2 kcal mol^{-1}. This would be of the order of disrupting a reasonable fraction of the intramolecular hydrogen bonds in PAM.

The quantitative determinations required to decide the correct mechanism would involve a simultaneous mapping of the birefringence magnitude and the strain rate. Also, in order to make a comparison with theoretical predictions of the birefringence of deformed coils, account would have to be made of the effect of transit time on elongation ratio. This effect of transit time on macromolecular deformation and orientation has been discussed by Leal *et al.*[3].

ACKNOWLEDGEMENTS

The expert photographic assistance of Mr Bruce Hibbs is gratefully acknowledged. Discussions with Professor R. K. Prud'homme, E. Samulski and Dr W. S. Yen were invaluable to the development of this work.

REFERENCES

1 Keller, A. and Odell, J. A. *Colloid Polym. Sci.* 1985, **263**, 181
2 Cressely, R. and Hocquart, R. in 'Rheology' (Eds. G. Astarita, G. Marrucci and L. Nicolais), 1980, Vol. 2, pp. 377–83
3 Leal, L. G., Fuller, G. G. and Olbricht, W. L. *Prog. Astro. Aero., Viscous Flow Drag Reduction* 1980, **72**, 351
4 Scrivener, O., Berner, C., Cressely, R., Hocquart, R., Sellin, R. and Vloches, N. S. *J. Non-Newtonian Fluid Mech.* 1979, **5**, 475
5 Mackley, M. R. and Keller, A. *Phil. Trans. R. Soc. Lond.* (*A*) 1975, **278**, 29
6 Farrell, C. J., Keller, A., Miles, M. J. and Pope, D. P. *Polymer* 1980, **21**, 1292
7 Miles, M. J., Tanaka, K. and Keller, A. *Polymer* 1983, **24**, 1081
8 Odell, J. A., Atkins, E. D. T. and Keller, A. *J. Polym. Sci., Polym. Lett. Edn.* 1983, **21**, 289
9 Odell, J. A., Keller, A. and Miles, M. J. *Polymer* 1985, **26**, 1219
10 Pope, D. P. and Keller, A. *Colloid Polym. Sci.* 1978, **256**, 751
11 Odell, J. A. and Keller, A. *J. Polym. Sci., Polym. Phys. Edn.* 1986, **24**, 1889
12 Odell, J. A., Keller, A. and Miles, M. J. *Polym. Commun.* 1983, **24**, 7
13 Peiffer, D. G., Kim, M. W. and Lundberg, R. D. *Polymer* 1986, **27**, 493
14 Hinch, E. J. *Phys. Fluids* 1977, **20** (10), Pt 11, S22
15 Rabin, Y., Henyey, F. S. and Pathria, R. K. *Phys. Rev. Lett.* 1985, **55** (2), 201
16 Henyey, F. S. and Rabin, Y. *J. Chem. Phys.* 1985, **82** (9), 4362
17 Farinato, R. S. *Polymer* 1988, **29**, 160
18 Fredericq, E. and Houssier, C. 'Electric Dichroism and Electric Birefingence', Clarendon Press, Oxford, 1973

19 Klein, J. and Conrad, K.-D. *Makromol. Chem.* 1978, **179**, 1635; McCarthy, K. J., Burkhardt, C. W. and Parazak, D. P. *J. Appl. Polym. Sci.* 1987, **33**, 1699
20 Gardner, K., Pike, E. R., Miles, M. J., Keller, A. and Tanaka, K. *Polymer* 1982, **23** (10), 1435
21 Farinato, R. S. unpublished results, 1987
22 Cressely, R., Hocquart, R., Decruppe, J.-P. and Wydro, T. Proc. *Microsymp. Macromol. 27th*, Walter de Gruyter, Berlin, 1985, pp. 507–10
23 Klein, J. and Scholz, W. *Makromol. Chem.* 1979, **180**, 1477
24 Kulicke, W.-M. and Kniewske, R. *Makromol Chem.* 1980, **181**, 823
25 Kulicke, W.-M. and Kniewske, R. *Makromol. Chem.* 1981, **182**, 2277
26 Leca, M. *Polym. Bull.* 1986, **16**, 537
27 Tsvetkov, V. N. in 'Newer Methods of Polymer Characterization' (Ed. K. Bacon), Interscience, New York, 1964
28 Dupuis, D., Layec, Y. and Wolff, C. in 'Optical Properties of Polymer Solutions' (Ed. G. H. Meeten), Elsevier, Amsterdam, 1986, Ch. 3
29 Tsvetkov, V. N. and Andreeva, L. N. *Adv. Polym. Sci.* 1981, **39**, 95
30 Kuhn, W. and Grun, G. *Kolloid Z.* 1942, **101**, 248
31 Tsvetkov, V. N., Frisman, E. V., Ptitsyn, O. B. and Kotliar, S. Ia. *Sov. Phys.–Tech. Phys.* 1958, **3**, 1325
32 Kuhn, W., Oswald, H. and Kuhn, H. *Helv. Chim. Acta* 1953, **36**, 1209
33 Brandup, J. and Immergut, E. H. (Eds.), 'Polymer Handbook', 2nd Edn., Wiley, New York, 1975
34 Hirschfelder, J. O., Curtiss and Bird, R. B. 'Molecular Theory of Gases and Liquids', Wiley, New York, 1954
35 Le Fevre, R. J. W. *Adv. Phys. Org. Chem.* 1965, **3**, 1
36 Kulicke, W.-M., Kniewske, R. and Klein, J. *Prog. Polym. Sci.* 1982, **8**, 373
37 Henyey, F. S. and Rabin, Y. *J. Chem. Phys.* 1985, **82** (9), 4362
38 Dash, J. W., Henyey, F. S. and Rabin, Y. *Physico-Chemical Hydrodynamics* 1985, **6** (5/6), 555